

# Inferring ecological interactions from time series data using neural ordinary differential equations fitted by Bayesian neural gradient matching

Willem Bonnaffé<sup>1,2</sup>, Ben Sheldon<sup>1</sup>, & Tim Coulson<sup>2</sup>

1. Edward Grey Institute of Field Ornithology, Department of Zoology, Oxford University, Zoology Research and Administration Building, 11a Mansfield Road, Oxford OX1 3SZ

2. Ecological and Evolutionary Dynamics Lab, Department of Zoology, Oxford University, Zoology Research and Administration Building, 11a Mansfield Road, Oxford OX1 3SZ

**Emails:** willem.bonnafe@stx.ox.ac.uk; tim.coulson@zoo.ox.ac.uk

**Running title:** Repeatable interactions and dynamics

**Keywords:** Artificial Neural Networks; Ecological Dynamics; Ecological interactions; Geber Method; Neural Ordinary Differential Equations; Ordinary Differential Equations; Prey-predator dynamics; Time series analysis; Rotifers; Microcosm;

**Specifications:** 140 words in abstract; 7071 words in text; 40 references; 5 figures; 1 table

**Contact:** Willem Bonnaffé, 61 St Giles, Pusey House, St Cross College, Oxford, OX1 3LZ, UK (w.bonnafe@gmail.com)

**Statement of authorship:** Willem Bonnaffé designed the method, performed the analysis, wrote the manuscript; Ben Sheldon provided input for the manuscript, commented on the manuscript. Tim Coulson led investigations, provided input for the manuscript, commented on the manuscript.

## **Abstract**

Generalisation of dynamical processes across natural systems is difficult because they are complex and hard to observe. The hope is that generalisation may be achieved by adequately modelling the complexity of systems, and observe them in sufficient detail. We investigate this by looking at the consistency of ecological interactions across three replicates of a three-species prey-predator system, well-observed in an artificial environment, using neural ordinary differential equations. We find that dominant interactions are consistent across the replicates, while weaker interactions are not, leading to different dynamical patterns across replicated systems. Our study hence suggests that generalisation of dynamical processes across systems may not be possible, even in simpler systems in ideal monitoring conditions. This is a problem because if we are not able to make generalisations in a simple artificial system, how can we make generalisation in the real world?

# 1 Introduction

The repeatability of ecological and evolutionary dynamics varies widely across systems and species. Sticklebacks from different lakes in Canada have independently evolved to a similar river morph phenotype (Thompson, Taylor, and Mcphail 1997). In guppies, four replicated populations located in different streams in Trinidad evolved the same low-predation phenotype (Reznick, Bryga, and Endler 1990). Multiple studies in experimental microcosms, particularly in rotifer populations, have shown that population dynamics were broadly repeatable (Yoshida et al. 2003; Yoshida et al. 2007; Becks et al. 2010; Becks et al. 2012; Hiltunen et al. 2013). Overall, this demonstrated that ecological and evolutionary dynamics may be repeatable across different instances of the same system, at least qualitatively. This was a fascinating finding given the complexity of the mechanisms involved and the subtle variations in environmental conditions across the different populations.

These systems hinted at the possibility for identifying global, generalisable, dynamical models. In practice, however, generalising dynamics and dynamical processes (i.e. functional representations describing which and how state variables affect each other and determine system dynamics) across natural systems has proven difficult (Lawton 1999). First, even if the dynamical patterns, and their outcomes, may appear to be conserved across similar systems, they may be underpinned by different processes. For instance, the evolution of the sticklebacks to highly similar river-adapted phenotypes has been shown to be underpinned by radically different genetic alterations (Raeymaekers et al. 2017). Second, it is often unclear whether quantitative differences across replicated systems

21 arise from pure stochasticity (Dallas et al. 2021), observation error (De Meester et al. 2019), or  
22 deterministic changes in the dynamical processes. Finally, the complexity of biological processes  
23 themselves (Adamson and Morozov 2013), differences in genetic and environmental contexts, may  
24 prevent the identification of a suitable dynamical model. For example, Becks and colleagues found  
25 that differences in the initial amount of genetic variation in otherwise identical rotifer populations  
26 led to subtle changes to the dynamics (Becks et al. 2010). Different access to seed supplies can  
27 modify the strength of the interaction between a plant and its herbivore, leading to either stable or  
28 oscillatory dynamics (Bonsall, Van Der Meijden, and Crawley 2003). Differences in temperature  
29 can alter the ecological interaction structure of entire ecosystems (Shurin et al. 2012; Bonnaffé  
30 et al. 2021). Because of this, vital rates are often found to be inconsistent in time (Gross, Ives, and  
31 Nordheim 2005; Adamson and Morozov 2013), and space (e.g. Gamelon et al. 2019). Overall, a  
32 growing body of evidence shows that generalisation of dynamical processes across similar natural  
33 systems often fails (Lawton 1999, e.g. Kendall et al. 2005; Demyanov, Wood, and Kedwards 2006;  
34 Ezard, Côté, and Pelletier 2009).

35 So how could repeatable dynamics arise across multiple instances of the same system? We would  
36 expect dynamics to be repeatable if the components of the system (e.g. species), as well as interac-  
37 tions between components, are conserved. For this, populations should have similar distributions  
38 for the traits that underpin these interactions, and should further share the same environmental con-  
39 ditions, across instances. While this is unreasonable to expect from a natural system, it may be  
40 achievable in an artificial setting. In such a setting, it is possible to understand the structure of

41 the system, to control the environment, and to reduce observation error. So if we fail to identify  
42 and generalise dynamical models in natural systems, perhaps we may be able to do so in artificial  
43 systems.

44 In spite of this there are few studies that have attempted to characterise the generalisability of  
45 dynamics across replicated systems in a laboratory setting. In such a setting, idiosyncrasies in pop-  
46 ulation dynamics can arise from (1) variations in ecological interactions and individual processes,  
47 as a result of evolution (e.g. Yoshida et al. 2003), or stochasticity (Dallas et al. 2021), (2) variations  
48 in initial conditions due to the experimental setting (Yoshida et al. 2003; Becks et al. 2010; De  
49 Meester et al. 2019), and (3) the complexity of the system which can lead to large changes in sys-  
50 tem dynamics with small changes in the system state and structure (Adamson and Morozov 2013).

51 Two studies, one in aphids and the other in rotifers, found substantial variation in vital rates across  
52 replicated populations, by fitting a stage-structured population ODE model to population dynamics  
53 time series data (Bruijning, Jongejans, and Turcotte 2019; Rosenbaum et al. 2019). These studies  
54 hint that generalisability of population dynamical processes may not be possible because of in-  
55 trinsic population structure and evolution, even in virtually identical populations hosted in artificial  
56 environments.

57 We identified three gaps in the literature. First, this kind of evidence remains scarce, due in part  
58 to the fact that dynamical modelling approaches guided by empirical data are still not widespread  
59 (Pontarp, Brännström, and Petchey 2019). Second, most of these studies relied on parametric  
60 frameworks, which impose arbitrary pre-determined forms for the dynamical processes at play, so

61 that their model may not capture properly the complexity of the dynamics of these populations (Jost  
62 and Ellner 2000; Adamson and Morozov 2013; Bonnaffé, Sheldon, and Coulson 2021). Finally,  
63 most studies usually analyse dynamics in single-species systems, but not multi-species systems,  
64 such as those with intraguild predation, which are more biologically realistic scenarios (Hiltunen  
65 et al. 2013). Further studies are consequently required to investigate the consistency of dynamical  
66 processes in simple multi-species and well-observed systems, to conclude about the generalisability  
67 of population dynamics across systems.

68 Our aim in this study is to provide an assessment of the repeatability of dynamical processes across  
69 different instances of a realistic multi-species system hosted in a well-observed environment. We  
70 do this by quantifying the direction, strength, and consistency of interactions in time and across  
71 replicates of a three-species microcosm in an experimental setting. We hypothesise that if the  
72 system is (1) simple enough, (2) well-observed, (3) in a controlled environment, then dynamical  
73 effects/interactions should be broadly consistent in time and across replicates, hence allowing for  
74 generalisation of dynamics across systems. We consider three replicates of a three-species system,  
75 consisting in a prey (algae), intermediate-predator (flagellate), and top-predator (rotifer). The algae  
76 is consumed by the flagellate and rotifer, and the flagellate is consumed by the rotifer. We use  
77 three replicated system runs from a study by Hiltunen and colleagues which feature sequential  
78 oscillations of the density of the three species (Hiltunen et al. 2013). We analyse the time series  
79 with neural ordinary differential equations (Bonnaffé, Sheldon, and Coulson 2021), which allows  
80 us to approximate non-parametrically population growth rates, and quantify the direction, strength,

81 and consistency of inter- and intra-specific effects on the growth of each population. We find that  
82 the interaction between the rotifer and algae is consistent throughout time and across replicates,  
83 while the interaction between the flagellate and the two other species is not. Our study suggests  
84 that dynamical processes may sometimes not be consistent and generalisable across systems, even  
85 when they are as close to identical as experimentation permits. We discuss these results and hint at  
86 the underlying impact of evolution driving differences in these systems.

87 In previous work, we developed a simulation-based approach to fit NODE systems to time series  
88 data (Bonnaffé, Sheldon, and Coulson 2021). We would first simulate the NODE system over  
89 the entire time series. Then we would compute the error between the predictions of the NODE  
90 model and the observations. Finally, we would change the weights of the NODEs to minimise  
91 this error. There are two caveats with this approach. The first caveat is that the NODE system  
92 has to be simulated over the entire range of the data at every step of the optimisation, which is  
93 computationally expensive to perform. Second, the numerical integration prevents the computation  
94 of gradients of the posterior distribution of the model, which prevents the use of efficient gradient  
95 descent approaches.

96 Ellner and colleagues introduced a technique called *gradient matching* to fit ODEs (Ellner, Seifu,  
97 and Smith 2002). The approach involves two steps. First, they interpolate the time series of each  
98 state variable with cubic splines to obtain interpolated states and dynamics. Second, they train  
99 each ODE to satisfy the interpolated state and dynamics. The interpolation allows them to bypass  
100 the simulation of the ODE system, and further makes the error function mathematically tractable,

101 allowing for the computation of gradients.

## 102 **2 Material and Methods**

### 103 **2.1 Method overview**

104 We aim to provide a nonparametric method for estimating ecological interactions from time series  
105 data of species density. We do this by approximating the dynamics of each species with neural  
106 ordinary differential equations (NODEs, Bonnaffé, Sheldon, and Coulson 2021). We then compute  
107 ecological interactions as the sensitivity of these dynamics to a change in the respective species  
108 densities.

### 109 **2.2 Neural ordinary differential equation**

110 A NODE is a class of ordinary differential equation (ODE) that is partly or entirely defined as an  
111 artificial neural network (ANN). They are useful to infer dynamical processes non-parametrically  
112 from time series data (Bonnaffé, Sheldon, and Coulson 2021). We choose NODEs over standard  
113 statistical approaches because they offer two advantages. The first is that NODEs approximate  
114 the dynamics of populations non-parametrically. NODEs are therefore not subjected to incorrect  
115 model specifications (Jost and Ellner 2000; Adamson and Morozov 2013). This provides a more  
116 objective estimation of the inter-dependences between state variables. The second advantage is that  
117 it is a dynamical systems approach. So that the approach includes lag effects through interacting  
118 state variables, not only direct effects between them.



119 We first consider a general NODE system,

$$\frac{dy_i}{dt} = f_p(y, \theta_i), \quad (1)$$

120 where  $dy_i/dt$  denotes the temporal change in the  $i^{th}$  variable of the system,  $y_i$ , as a function of the  
 121 other state variables  $y = \{y_1, y_2, \dots, y_I\}$ . The function  $f_p$  is a nonparametric function of the state  
 122 variables and its shape is controlled by the parameter vector  $\theta_i$ . In the context of NODEs, non-  
 123 parametric functions are ANNs. The most common class of ANN used in NODEs are single-layer  
 124 fully connected feedforward ANNs (e.g. Wu, Fukuhara, and Takeda 2005), also referred to by  
 125 single layer perceptrons (SLPs, Bonnaff  , Sheldon, and Coulson 2021),

$$f_p(y, \theta_i) = f_\lambda \left( \theta_i^{(0)} + \sum_{j=1}^J \theta_{ij}^{(1)} f_\sigma \left( \theta_{ij}^{(2)} + \sum_{k=1}^K \theta_{ijk}^{(3)} y_k \right) \right), \quad (2)$$

126 which feature a single layer, containing  $J$  neurons, that maps the inputs, here the state variables  $y$ ,  
 127 to a single output, the dynamics of state variable  $i$ ,  $dy_i/dt$ . The parameter vector  $\theta_i$  contains the  
 128 weights  $\theta^{(l)}$  of the connections in the SLPs. SLPs can be viewed as weighted sums of activation  
 129 functions  $f_\sigma$ , which are usually chosen to be *sigmoid* functions  $f(x) = 1/(1 + \exp(-x))$ . The link  
 130 function  $f_\lambda$  allows to map the output of the network to a specific domain, for instance applying  
 131 *tanh* will constrain the dynamics between -1 and 1,  $dy_i/dt \in ]-1, 1[$ .

### 132 2.3 Fitting NODEs by Bayesian neural gradient matching

133 In this section, we describe how to estimate the parameters  $\theta$  of the NODE system given a set of  
134 time series. Fitting NODEs can be highly computationally intensive, which hinders uncertainty  
135 quantification, cross-validation, and model selection (Bonnaffé, Sheldon, and Coulson 2021). We  
136 solve this issue by introducing *Bayesian neural gradient matching* (BNGM), a computationally  
137 efficient approach to fit NODEs. The approach involves two steps (Fig. 1). First, we interpolate the  
138 state variables and their dynamics with neural networks. Second, we train each NODE to satisfy  
139 the interpolated state and dynamics. This bypasses the costly numerical integration of the NODE  
140 system and provides a fully mathematically tractable expression for the posterior distribution of  
141 the parameter vector  $\theta$ . We coin the term BNGM to emphasise two important refinements of the  
142 standard gradient matching algorithm. The first is that we use neural networks as interpolation  
143 functions, and the second is that we use Bayesian regularisation to limit overfitting and estimate  
144 uncertainty around parameters.

#### 145 Interpolating the time series

146 The first step is to interpolate the time series and differentiate it with respect to time in order  
147 to approximate the state and dynamics of the variables. We perform the interpolation via non-  
148 parametric regression of the interpolating functions on the time series data,

$$Y_{it} = \tilde{y}_i(t, \omega_i) + \epsilon_{it}^{(o)}, \quad (3)$$

149 where  $Y_{it}$  is observed value of the state variable  $i$  at time  $t$ ,  $\tilde{y}_i(t, \omega_i)$  is the value predicted by the  
 150 interpolation function given the parameter vector  $\omega_i$ , and  $\varepsilon_{it}^{(o)}$  is the observation error between the  
 151 observation and prediction. The interpolation function is chosen to be a neural network,

$$\tilde{y}_i(t, \omega_i) = f_\lambda \left( \omega_i^{(0)} + \sum_{j=1}^J \omega_{ij}^{(1)} f_\sigma \left( \omega_{ij}^{(2)} + \omega_{ij}^{(3)} t \right) \right), \quad (4)$$

152 where the parameter vector  $\omega_i$  contains the weights  $\omega^{(l)}$  of the network. We can further differ-  
 153 entiate this expression with respect to time to obtain an interpolation of the dynamics of the state  
 154 variables,

$$\frac{d\tilde{y}_i}{dt}(t, \omega_i) = \sum_{j=1}^J \omega_{ij}^{(1)} \omega_{ij}^{(3)} \frac{\partial f_\sigma}{\partial t} \left( \omega_{ij}^{(2)} + \omega_{ij}^{(3)} t \right) \frac{\partial f_\lambda}{\partial t} \left( \omega_i^{(0)} + \sum_{k=1}^J \omega_{ik}^{(1)} f_\sigma \left( \omega_{ik}^{(2)} + \omega_{ik}^{(3)} t \right) \right). \quad (5)$$

### 155 **Fitting NODEs to the interpolated time series**

156 The second step is to train the NODE system (Eq. 1) to satisfy the interpolated dynamics. Thanks  
 157 to the interpolation step, this simply amounts to performing a non-parametric regression of each  
 158 NODE (Eq. 1) on the interpolated dynamics (Eq. 5),

$$\frac{\partial \tilde{y}_i}{\partial t}(t, \omega_i) = \frac{dy_i}{dt}(\tilde{y}, \theta_i) + \varepsilon_{it}^{(p)}, \quad (6)$$

159 where  $\varepsilon_{it}^{(p)}$  is the process error, namely the difference between the interpolated dynamics,  $\partial \tilde{y}_i / \partial t$   
 160 and the NODE,  $dy_i / dt$ , given the interpolated state variables  $\tilde{y} = \{\tilde{y}_1, \tilde{y}_2, \dots, \tilde{y}_I\}$ .

## 161 Bayesian regularisation

162 In the context of standard gradient matching, defining the observation model (Eq. 3) and process  
 163 model (Eq. 6) would be sufficient to fit the NODE system (Eq. 1) to the time series via optimisation.  
 164 We could find the parameter vector  $\omega_i$  and  $\theta_i$  that minimise the sum of squared observation and  
 165 process errors,  $\varepsilon_{it}^{(o)}$  and  $\varepsilon_{it}^{(p)}$  (Eq. 3 and 6). However, this approach is prone to overfitting, and does  
 166 not provide estimates of uncertainty around model predictions. To account for this, we introduce  
 167 Bayesian regularisation, which allows us to control for overfitting by constraining parameters with  
 168 prior distributions (Cawley and Talbot 2007), and to root our interpretation of uncertainty in a  
 169 statistically sound framework.

170 First, we define a simple Bayesian model to fit the interpolation functions (Eq. 3) to the time series  
 171 data. We assume normal distributions for the observation error,  $\varepsilon_{ij}^{(o)} \sim \mathcal{N}(0, \sigma_i)$ , and for the pa-  
 172 rameters,  $\omega_{ij} \sim \mathcal{N}(0, \gamma_{ij})$ . Here, we are only interested in interpolating the time series accurately,  
 173 irrespective of the value of  $\sigma_i$  and  $\gamma_{ij}$ . Therefore, we use the approach developed by Cawley and  
 174 Talbot to average out the value of the parameters  $\sigma_i$  and  $\gamma_{ij}$  in the full posterior distribution (Caw-  
 175 ley and Talbot 2007), assuming gamma hyperpriors  $p(\xi) \propto \frac{1}{\xi} \exp\{-\xi\}$  for both parameters. This  
 176 yields the following expression for the log marginal posterior density of the parameters,

$$\log P(\omega_i | Y_i) \propto -\frac{J}{2} \log \left( 1 + \sum_{j=1}^J \left( \varepsilon_{ij}^{(o)} \right)^2 \right) - \frac{K}{2} \log \left( 1 + \sum_{k=1}^K \omega_{ik}^2 \right) \quad (7)$$

177 where  $P$  is the marginal posterior density,  $\omega_i = \{\omega_{i1}, \omega_{i2}, \dots, \omega_{iK}\}$  is the observation parameter  
 178 vector controlling the interpolation function,  $Y_i = \{Y_{i1}, Y_{i2}, \dots, Y_{iJ}\}$  corresponds to the sequence of

179 observations of state variable  $i$  at time step  $j$ ,  $J$  is the total number of time steps in the time series,  
 180  $\varepsilon_{ij}^{(o)}$  is the observation error at time step  $j$  between the interpolated and observed value of variable  
 181  $i$ ,  $K$  is the total number of parameters. More details on how to derive this expression can be found  
 182 in a supplementary file (Supplementary A).

183 Then, we define a simple Bayesian model to fit the NODEs to the interpolated dynamics, given the  
 184 interpolated states. We assume normal distributions for the observation error,  $\varepsilon_{ij}^{(p)} \sim \mathcal{N}(0, \sigma_i)$ , and  
 185 parameters,  $\theta_{ik} \sim \mathcal{N}(0, \delta_{ik})$ . This gives the following expression for the log posterior density of  
 186 the parameters given the interpolations,

$$\log p(\theta_i | \omega) \propto -\frac{1}{2} \sum_{j=1}^J \left( \frac{\varepsilon_{ij}^{(p)}}{\sigma_i} \right)^2 - \frac{1}{2} \sum_{k=1}^K \left( \frac{\theta_{ik}}{\delta_{ik}} \right)^2 \quad (8)$$

187 where  $\theta_i = \{\theta_{i1}, \theta_{i2}, \dots, \theta_{iK}\}$  are the NODE parameters of the  $i^{th}$  variable,  $\omega = \{\omega_1, \omega_2, \dots, \omega_I\}$  are  
 188 the interpolation parameters of each state variable,  $\varepsilon_{ij}^{(p)}$  is the process error of variable  $i$  at time  
 189 step  $j$  between the interpolated dynamics and NODE prediction,  $\sigma_i$  is the standard deviation of the  
 190 likelihood,  $K$  is the total number of parameters,  $\delta_{ik}$  is the standard deviation of the prior distribution  
 191 of parameter  $\theta_{ik}$ .

192 This approach allows us to limit overfitting by adjusting the constraint on the parameters, which  
 193 is controlled by the standard deviation of the parameter prior distributions,  $\delta_{ik}$  (Cawley and Talbot  
 194 2007; Bonnaffé, Sheldon, and Coulson 2021). This can be used to control the degree of non-  
 195 linearity in the response, but also to eliminate specific variables from the model by constraining  
 196 their parameters to be close to zero. We identify the appropriate degree of constraint  $\delta_i$  on NODE

197 parameters via cross-validation. We train the NODE model on the first half of the interpolated data  
198 and predict the remaining half. We repeat this process for increasing values of  $\delta_i$ , until we find the  
199 value that maximises the log likelihood of the test data.

## 200 **2.4 Inference and uncertainty quantification**

201 Finally, we estimate uncertainty in parameter values by *anchored ensembling*, which produces  
202 approximate Bayesian estimates of the posterior distribution of the parameters (Pearce et al. 2018).  
203 The technique requires sampling a parameter vector from the prior distributions,  $\theta_i \sim \mathcal{N}(0, \delta_i)$ ,  
204 and then optimising the posterior distribution from this starting point,  $\theta_i^* = \underset{\theta_i}{\operatorname{argmax}} \log p(\theta_i \mid \omega)$ .  
205 By repeatedly taking samples, the sampled distribution  $\theta^*$  approaches the posterior distribution  
206 and provides estimates and error around the quantities that can be derived from the models. The  
207 expectation and uncertainty around derived quantities can then be obtained by computing the mean  
208 and variance of the approximated posterior distributions. The great strength of this approach is  
209 that it is unlikely to get stuck in local maxima and provides a more robust optimisation of the  
210 posterior.

## 211 **2.5 Analysing NODEs**

212 In this study we are mainly interested in two outcome of NODEs, namely inferring the direction  
213 (or effect) and strength (or contribution) of interactions between the state variables (Bonnaiffé,  
214 Sheldon, and Coulson 2021). We define the direction of the interaction between variable  $y_i$  and  $y_j$   
215 as the derivative of the dynamics of  $y_j$  with respect to  $y_i$ , and vice versa,

$$e_{ijt} = \frac{\partial}{\partial y_j} \frac{dy_i}{dt}. \quad (9)$$

216 Knowing the direction, however, is not sufficient to determine the importance of a variable for the  
 217 dynamics of another. Given the same effects, a variable that fluctuates a lot will have a greater  
 218 impact on the dynamics of a focal variable, compared to a variable that remains quasi-constant. We  
 219 hence compute the strength of the interaction by multiplying the dynamics of a variable  $y_j$  by its  
 220 effect on the focal variable  $y_i$ , also known as the Geber method (Hairston et al. 2005),

$$c_{ijt} = \frac{dy_j}{dt} \frac{\partial}{\partial y_j} \frac{dy_i}{dt}. \quad (10)$$

221 To summarise results across the entire time series we can compute the mean effects  $e_{ij}$  by averaging  
 222  $e_{ijt}$  across the entire time series,  $e_{ij} = K^{-1} \sum_k e_{ijk}$ , as well as the relative total contribution,  $c_{ij}$ ,  
 223 of a variable to the dynamics of another by computing the relative sum of square contributions,  
 224  $c_{ij} = \left( \sum_{jk} c_{ijk}^2 \right)^{-1} \sum_t c_{ijt}^2$ . By computing the direction and strength of interactions between all the  
 225 variables in the system we can build dynamically informed ecological interaction networks (See  
 226 case study below for examples). Other metrics can be computed by analysing the NODEs, such  
 227 as equilibrium states, these are discussed in our previous work (Bonnaffé, Sheldon, and Coulson  
 228 2021).

## 229 **3 Case study 3: rotifer, algae, and flagellate**

### 230 **3.1 System**

231 We consider a three-species laboratory microcosm consisting of an algal prey (*Chlorella autroph-*  
232 *ica*), a flagellate intermediate predator (*Oxyrrhis marina*), and a rotifer top predator (*Brachionus*  
233 *plicatilis*). The algal prey is consumed by the intermediate and top predator, the top predator also  
234 consumes the intermediate predator (Arndt 1993). The dynamics of this system, here the daily  
235 change in the density of each species, were recorded in three replicated time series experiments  
236 performed by Hiltunen and colleagues (Hiltunen et al. 2013, Fig. 1).

237 We use their time series because they describe a simple yet biologically realistic ecosystem, and  
238 because the quality of the replication of their microcosm reduces as much as possible observational  
239 and experimental error, and rules out environmental variation (Hiltunen et al. 2013). We digitised  
240 these time series by extracting by hand the coordinates of every points in the referential of the axis  
241 of the graph of the original study, and analysed them.

### 242 **3.2 Model specifications**

243 The aim of the modelling approach is to infer the drivers of the dynamics of each species from  
244 the time series data. More specifically, we want to quantify the effect of a change in the density  
245 of one species on the growth rate of the other species. We define a simple NODE system for the  
246 three-species system described previously,



$$\begin{aligned}
\frac{dR}{dt} &= r_R(R, G, B, \beta_R)R \\
\frac{dG}{dt} &= r_G(R, G, B, \beta_G)G \\
\frac{dB}{dt} &= r_B(R, G, B, \beta_B)B,
\end{aligned} \tag{11}$$

247 where  $dR/dt$ ,  $dG/dt$ , and  $dB/dt$  denote the change in rotifer ( $R$ ), algae ( $G$ ), and flagellate ( $B$ )  
 248 density in continuous time. The per-capita growth rates  $r_R$ ,  $r_G$ , and  $r_B$  are non-parametric functions  
 249 of the density  $R$ ,  $G$ ,  $B$  of each species,

$$r_R = \sum_{i=1}^N \beta_i f_{\sigma}(\beta_{i0} + \beta_{i1}R + \beta_{i2}G + \beta_{i3}B) \tag{12}$$

250 where the parameter vectors  $\beta_R$ ,  $\beta_G$ , and  $\beta_B$ , control the shape of the growth rates.

## 251 **4 Results**

252 We analyse sequentially the dynamics of each species, focussing on the amount of variation in  
 253 per-capita growth rates explained by the NODE model, the overall direction, consistency, and im-  
 254 portance of ecological interactions, and differences across replicates. Results are summarised in  
 255 Table 1 and described in details for each species in the following section.

### 256 **Drivers of top predator dynamics**

257 Figure 2 presents the drivers of the dynamics of rotifer. The NODE approximation of the per-capita  
 258 growth rate fits quite well the interpolated per-capita growth rate across all replicates (Fig. 2, A2

259 B2 and C2,  $r^2 > 0.7$ , Table 1). The analysis of effects reveals overall a positive effect of algae on  
 260 rotifer growth in all replicates (Fig. 2, A3, B3, C3, green line). The intermediate predator has a  
 261 positive effect on rotifer growth in replicates A and C only (Fig. 2, A3, B3, C3, blue line). We find  
 262 positive intra-specific density-dependence in the first replicate only (Fig. 2, A3, red line). Overall,  
 263 all effects are consistent throughout the time series. The algae is the dominant driver of rotifer  
 264 dynamics as it accounts for 55%, 93%, and 74% of the change in per-capita growth rates across the  
 265 three replicates (Table 1, Fig. 2, A5, B5, C5, green line).

#### 266 **Drivers of the prey dynamics**

267 The per-capita growth rate of the algae is well explained by the NODE approximation (Fig. 3,  
 268 A2, B2, C2,  $r^2 > 0.8$ , Table 1). Overall, rotifers have a negative impact on the growth of algae  
 269 in all replicates (Fig. 3, A3, B3, C3, red line). We find evidence for negative density-dependence  
 270 in replicate A and positive density-dependence in replicate B, but not in replicate C (Fig. 3, A3,  
 271 B3, C3, green line). The intermediate predator has an overall negative effect on Algae only in  
 272 replicate B (Fig. 3, B3, blue line). The main driver of algae dynamics is the rotifer population,  
 273 which accounts for 58%, 44%, and 90% of the change in algae per-capita growth rate across the  
 274 three replicates. Density-dependence, however, plays a role in replicate A and B, with 40% and  
 275 24% of total change in growth, respectively (Table 1). The intermediate predator contributes only  
 276 to algae growth in replicate B, accounting for 32% change in growth (Table 1). Overall, effects are  
 277 found to be consistent throughout the time series except in replicate B (Fig. 3, B3), where effects  
 278 vary in complicated ways, leading to a period in the time series where the algae is mostly driven by

279 the intermediate predator and positive density-dependence, and less impacted by the top predator  
280 (Fig. 3, B5, from time 3 to 7.5).

## 281 **Drivers of the intermediate predator dynamics**

282 The per-capita growth rate of the intermediate predator is quite well captured by the NODE approx-  
283 imation (Fig. 4, A2, B2, C2,  $r^2 > 0.7$ , Table 1). The intermediate predator is mainly negatively  
284 affected by the rotifer population (Fig. 4, A3, B3, C3, red line). The algae has a negative effect  
285 on flagellate growth in replicate A, and a positive one in replicate B (Fig. 4, A3, B3, green line).  
286 The rotifer predator dynamics accounts for 78%, 62%, 91% of the change in the flagellate growth  
287 rate, and the algae 20% and 37% in replicate A and B, respectively (Table 1, Fig. 4, A5, B5, C5).  
288 Overall, effects are consistent throughout the time series.

## 289 **5 Discussion**

290 Our ability to generalise dynamical processes and patterns across populations and communities is  
291 limited by the complexity of the processes, differences in environments, and incomplete and/or  
292 erroneous observations. It remains unclear to what extent generalisation would be possible if we  
293 overcame these limitations. We tackle this question by looking at the consistency of dynamical  
294 patterns across three replicated runs of a simple three-species community, hosted in identical en-  
295 vironmental conditions in the lab. We expected to find consistency in the drivers of population  
296 dynamics, both in time and across replicates, and thereby demonstrate that generalisation of dy-  
297 namical processes may be possible if the system states were well-observed and environmental

conditions were known. To verify this expectation we (1) characterised the amount of variation in per-capita growth rates that is explainable deterministically, (2) quantified the direction, strength, and importance of ecological interactions for the growth of each population, and (3) described how these varied in time and across replicates. Our results are summarised in Figure 5. We find that only the effect of algae on rotifer ( $G \rightarrow R$ ), and that of rotifer on algae ( $R \rightarrow G$ ) and flagellate ( $R \rightarrow B$ ) are conserved across the replicates. We find strong variation in the direction and importance of intra-specific density-dependence in rotifer ( $R \rightarrow R$ ) and algae ( $G \rightarrow G$ ) growth across the three replicates. The role played by the intermediate predator in the system was also different in all replicates, in that it only contributed substantially to the dynamics of the algae in replicate B ( $B \rightarrow G$ ), and was either negatively, positively, or not affected by the algae ( $G \rightarrow B$ ). Overall, this shows that the dominant interactions are conserved across replicates, but that minor interactions vary substantially in importance and effect. Furthermore, we find that these dynamical processes are more consistent in time within a system, than across replicates. Our results demonstrate that because of partially generalisable dynamical processes, dynamical patterns may not be generalisable across systems, even with limited observation error and when environmental conditions and community structure are conserved.

Overall, our results are consistent with the biology of the system. The rotifer top-predator is found to have a strong negative impact on the two other species, in spite of variation in prey preference across replicates. This is consistent with previous study which have established the importance of rotifers for top-down control of flagellate and algal populations (Arndt 1993; Hiltunen et al.

2013). What is more surprising is the positive intra-specific density-dependence in the growth rate of the rotifer population in replicate A. This implies that the population of rotifer grows more at high density. This might be explained by various biological mechanisms, such as cannibalism (Gilbert 1976), though evidence remains limited in the *Brachionus* genus, or higher mating success at high density (Snell and Garman 1986). Similarly, the algae shows signs of positive intra-specific density-dependence in replicate B, though this effect remains confined to a brief period in the time series. This may be due to a higher chance of evading predators at high-density. This shows that the NODEs approach used here recovers results consistent with existing knowledge, but also identify subtle, more intriguing dynamical processes.

What might be the drivers of differences in the dynamical processes across these three replicates? One of the main source of variation in dynamics may be differences in the intrinsic structure of populations, such as variation in traits influencing intra- and inter-specific interactions which may lead to different dynamics (Yoshida et al. 2003; Yoshida et al. 2007; De Meester et al. 2019; Bruijning, Jongejans, and Turcotte 2019). Differences in the phenotypic structure may be due to unaccounted variation in initial conditions (Becks et al. 2010), or variation that developed throughout time as a result of evolution (e.g. Yoshida et al. 2003; Yoshida et al. 2007). In particular, the algae in this system is prone to evolve a predator defence behaviour, by forming clumps, which reduce predation risk (Yoshida et al. 2003; Hiltunen et al. 2013). In their original paper, the authors limited the initial genetic diversity in the algae and focussed on replicates which did not display evidence of evolution, in an attempt to limit the impact of initial variation in phenotypic structure,

338 and of evolution, on the dynamics (Hiltunen et al. 2013). In spite of that, evolution may not be  
339 eliminated completely, thus variation in traits governing the interactions between the species in  
340 the system may still have developed during the experiment, and led to changes in the dynamical  
341 processes across replicates. This would further be consistent with results from Yoshida and col-  
342 leagues, who showed that evolution of prey defense could lead to ecological dynamics inconsistent  
343 with the known trophic interactions (Yoshida et al. 2007). Becks and colleagues also showed that  
344 small changes in the initial genotypic diversity could lead to drastically different eco-evolutionary  
345 dynamics (Becks et al. 2010). Our study hence reinforces the idea that rapid evolution may prevent  
346 generalisation of dynamical processes (Ezard, Côté, and Pelletier 2009; De Meester et al. 2019),  
347 and further suggests that this may also be the case in simple systems with limited environmental  
348 variation and opportunity for evolution.

349 Alternatively, stochasticity may be a major driver of differences across systems (Dallas et al. 2021).  
350 First, stochasticity in initial conditions, arising from the sampling of the communities of each  
351 replicate, could introduce differences in the interactions between the three populations. Second,  
352 stochasticity in the population dynamics themselves may result in different changes in density lev-  
353 els in communities that are otherwise identical. Because our modelling approach is deterministic,  
354 it does not directly provide an estimate of the total variation explained by stochasticity. Our mod-  
355 elling approach decomposes the variation in the data into observation and process error (Calder et  
356 al. 2003). First, the interpolation step introduces residual observation error, namely variation that  
357 is not captured by the interpolation. Second, the fitting of the NODE to the interpolation introduces

358 residual process error, which is variation in the observation model that is not explained by the pro-  
359 cess modelled by the NODE. Stochasticity in the dynamics could explain the observation and pro-  
360 cess residual error (Calder et al. 2003), while stochasticity in initial conditions can only influence  
361 differences across replicates. Yet, we find relatively small process and observation error ( $> 70\%$   
362 of variance explained). So that, the dynamics of the three species are well explained by relatively  
363 simple linear deterministic effects between the state variables, which means that though dynamical  
364 processes differ across replicates they are reasonably consistent in time within each system. This  
365 suggests that stochasticity in dynamics plays a minor role in driving differences in dynamics across  
366 replicates, compared to stochasticity in initial conditions. In order to quantify this, we would need  
367 to estimate the influence of stochasticity directly. This can be done by modelling explicitly the  
368 random distribution of model parameters that underpin the dynamics of populations, which would  
369 then inform us about the importance of stochasticity driven by variation at the individual-level (Fox  
370 and Kendall 2002). Additionally, we could model stochasticity explicitly in the model with neural  
371 stochastic differential equations, which would allow us to separate the amount of change explain-  
372 able by the deterministic part of the model, from demographic stochasticity, at each time step (Jia  
373 and Benson 2019).

374 Finally, we cannot exclude the potential contribution of unobserved variables that were not moni-  
375 tored during the experiment, such as variation in nutrient levels in the chemostat, and which may  
376 also lead to differences in the predation and intra-specific interactions across systems (e.g. Bonsall,  
377 Van Der Meijden, and Crawley 2003; Fussmann and Blasius 2005; Posey, Alphin, and Cahoon

378 2006).

379 Should we expect limited generalisability of dynamics across systems, even if the complexity of  
380 the process is properly captured, environmental conditions known, and the system well-observed?

381 A similar study, that inferred dynamical processes consistency from replicated time series of a  
382 simple rotifer system, found substantial variation in vital rates across replicates (Rosenbaum et al.  
383 2019), also pointing at a low generalisability of dynamical processes. Yet, the level of replication  
384 of the time series of their studies was not as stringent as that of the time series we considered,  
385 which leaves room for variability in dynamics to be caused by differences in experimental setup,  
386 population history, initial densities. Bruijning and colleagues also found substantial variation in  
387 vital rates across clones in a replicated system of aphids, showing that slight phenotypic variations  
388 can change the population dynamics, all else being equal (Bruijning, Jongejans, and Turcotte 2019).

389 This phenomenon is likely to be even more important in more complicated systems and in a natural  
390 setting where most variables are unobserved, which poses a problem for the generalisation of results  
391 across studies and systems (De Meester et al. 2019). How can we expect to generalise dynamics  
392 across real systems if we are not able to do so in artificial systems? Overall, our study reinforces  
393 the view that general inferences should not be drawn from a single system, and that more efforts  
394 are required to distinguish dynamical patterns that are conserved across systems from idiosyncratic  
395 ones.

396 Can we trust our models then if they are doomed to provide partly idiosyncratic answers? Our  
397 study demonstrates that processes can vary substantially across replicates, so that there may hence



398 not be a single suitable functional form and parametrisation to model them (Lawton 1999). Yet,  
399 most of the work to date has involved fitting parametric models to time series data (e.g. Bruijning,  
400 Jongejans, and Turcotte 2019; Pontarp, Brännström, and Petchey 2019; Rosenbaum et al. 2019),  
401 which provide a very narrow view of the range of possible functions to describe the biological  
402 processes at play (Jost and Ellner 2000; Adamson and Morozov 2013). These models are subjective  
403 by nature (Jost and Ellner 2000; Adamson and Morozov 2013), and hence not generalisable, so that  
404 they greatly reduce our chance at identifying dynamical processes that are idiosyncratic, and those  
405 that are transferable.

406 What alternatives do we have then? We propose that NODEs are a suitable framework to study  
407 dynamical processes, as they produce inferences that are free of model assumption and facilitate  
408 comparison across studies and systems (Bonnaiffé, Sheldon, and Coulson 2021). In this sense, our  
409 study already provides a potentially more objective depiction of dynamical processes than previous  
410 work with parametric models. Furthermore, in this paper we overcame the practical challenges  
411 of implementing NODEs by providing a computationally efficient fitting procedure, relying on  
412 time series interpolation, and developed a model selection criterion robust to overfitting. Similar  
413 approaches have been proposed in the past, for instance Ellner and colleagues developed a method  
414 called gradient matching where they interpolated the data with cubic splines to which they fitted  
415 the differential equations (Jost and Ellner 2000; Ellner, Seifu, and Smith 2002). Wu and colleagues  
416 also relied on data interpolation of the data with ANNs to fit non-parametric approximations of  
417 population vital rates (Wu, Fukuhara, and Takeda 2005). But the approaches were too challenging

418 and cumbersome to be implemented routinely, and were not used to tackle ecological interactions.  
419 Overall, our work demonstrates the usefulness of NODEs for inferring ecological interactions from  
420 count time series, which could readily be applied to a substantial pool of time series data.

## 421 **Conclusion**

422 Generalising dynamics across biological systems is hard because of the complexity of the dynam-  
423 ical processes (e.g. ecological interactions), differences in environmental context, and monitoring  
424 limitations. It remains unclear whether we could generalise dynamics if we properly modelled  
425 complexity, controlled for environmental effects, and observed systems precisely. We addressed  
426 this question by looking at the generalisability of dynamical processes across three replicated time  
427 series of a three-species system, using the novel framework of NODEs. We found that only the  
428 dominant interactions were conserved across the three time series, namely that between the algae  
429 and the rotifer, while the role of the intermediate predator varied substantially. Our results hence  
430 suggest that generalisation may not seem possible, even in simple system with no environmental  
431 variation. Given previous work in this system, the main cause of differences across replicates may  
432 be evolution in prey defence traits. We conclude that more work is required, using NODEs, to  
433 identify dynamical patterns that are conserved and those that are idiosyncratic across a wider range  
434 of systems.

## 435 **Acknowledgments**

436 We thank warmly the Ecological and Evolutionary Dynamics Lab and Sheldon Lab Group at the  
437 department of Zoology for their feedback and support. We thank Ben Sheldon for insightful sug-

gestions on early versions of the work. The work was supported by the Oxford-Oxitec scholarship and the NERC DTP.

#### **Data accessibility**

All data and code will be made fully available at <https://github.com/WillemBonnaffe/NODER/rotifer>.

#### **Statement of authorship**

Willem Bonnaffé designed the method, performed the analysis, wrote the manuscript; Tim Coulson led investigations, provided input for the manuscript, commented on the manuscript.

#### **References**

- Adamson, M. W. and A. Y. Morozov (2013). “When can we trust our model predictions? Unearthing structural sensitivity in biological systems”. In: *Proceedings of the Royal Society A: Mathematical, Physical and Engineering Sciences* 469.2149, pp. 1–19.
- Arndt, H. (1993). “Rotifers as predators on components of the microbial web (bacteria, heterotrophic flagellates, ciliates) - a review”. In: *Hydrobiologia* 255-256.1, pp. 231–246.
- Becks, L., S. P. Ellner, L. E. Jones, and N. G. J. Hairston (2010). “Reduction of adaptive genetic diversity radically alters eco-evolutionary community dynamics”. In: *Ecology Letters* 13.8, pp. 989–997.

454 Becks, L., S. P. Ellner, L. E. Jones, and N. G. J. Hairston (2012). “The functional genomics of  
 455 an eco-evolutionary feedback loop: Linking gene expression, trait evolution, and community  
 456 dynamics”. In: *Ecology Letters* 15.5, pp. 492–501.

457 Bonnaiffé, W., A. Danet, S. Legendre, and E. Edeline (2021). “Comparison of size-structured and  
 458 species-level trophic networks reveals antagonistic effects of temperature on vertical trophic  
 459 diversity at the population and species level”. In: *Oikos* 130.8, pp. 1297–1309.

460 Bonnaiffé, W., B. C. Sheldon, and T. Coulson (2021). “Neural ordinary differential equations for  
 461 ecological and evolutionary time series analysis”. In: *Methods in Ecology and Evolution* 2, pp. 1–  
 462 46.

463 Bonsall, M. B., E. Van Der Meijden, and M. J. Crawley (2003). “Contrasting dynamics in the same  
 464 plant-herbivore interaction”. In: *Proceedings of the National Academy of Sciences of the United  
 465 States of America* 100.25, pp. 14932–14936.

466 Bruijning, M., E. Jongejans, and M. M. Turcotte (2019). “Demographic responses underlying eco-  
 467 evolutionary dynamics as revealed with inverse modelling”. In: *Journal of Animal Ecology* 88.5,  
 468 pp. 768–779.

469 Calder, C., M. Lavine, P. Müller, and J. S. Clark (2003). “Incorporating multiple sources of stochas-  
 470 ticity into dynamic population models”. In: *Ecology* 84.6, pp. 1395–1402.

471 Cawley, G. C. and N. L. C. Talbot (2007). “Preventing over-fitting during model selection via  
 472 bayesian regularisation of the hyper-parameters”. In: *Journal of Machine Learning Research* 8,  
 473 pp. 841–861.

474 Dallas, T., B. A. Melbourne, G. Legault, and A. Hastings (2021). “Initial abundance and stochas-  
 475 ticity influence competitive outcome in communities”. In: *Journal of Animal Ecology*, pp. 1–  
 476 26.

477 De Meester, L. et al. (2019). “Analysing eco-evolutionary dynamics—The challenging complexity  
 478 of the real world”. In: *Functional Ecology* 33.1, pp. 43–59.

479 Demyanov, V., S. N. Wood, and T. J. Kedwards (2006). “Improving ecological impact assessment  
 480 by statistical data synthesis using process-based models”. In: *Journal of the Royal Statistical*  
 481 *Society. Series C: Applied Statistics* 55.1, pp. 41–62.

482 Ellner, S. P., Y. Seifu, and R. H. Smith (2002). “Fitting Population Dynamic Models to Time-Series  
 483 Data by Gradient Matching”. In: *Ecology* 83.8, p. 2256.

484 Ezard, T. H. G., S. D. Côté, and F. Pelletier (2009). “Eco-evolutionary dynamics: Disentangling  
 485 phenotypic, environmental and population fluctuations”. In: *Philosophical Transactions of the*  
 486 *Royal Society B: Biological Sciences* 364.1523, pp. 1491–1498.

487 Fox, G. A. and B. E. Kendall (2002). “Demographic stochasticity and the variance reduction ef-  
 488 fect”. In: *Ecology* 83.7, pp. 1928–1934.

489 Fussmann, G. F. and B. Blasius (2005). “Community response to enrichment is highly sensitive to  
 490 model structure”. In: *Biology Letters* 1.1, pp. 9–12.

491 Gamelon, M. et al. (2019). “Accounting for interspecific competition and age structure in demo-  
 492 graphic analyses of density dependence improves predictions of fluctuations in population size”.  
 493 In: *Ecology Letters* 22.5, pp. 797–806.

494 Gilbert, J. J. (1976). “Selective cannibalism in the rotifer *Asplanchna sieboldi*: Contact recognition  
 495 of morphotype and clone”. In: *Proceedings of the National Academy of Sciences* 73.9, pp. 3233–  
 496 3237.

497 Gross, K., A. R. Ives, and E. V. Nordheim (2005). “Estimating fluctuating vital rates from time-  
 498 series data: A case study of aphid biocontrol”. In: *Ecology* 86.3, pp. 740–752.

499 Hairston, N. G. J., S. P. Ellner, M. A. Geber, T. Yoshida, and J. A. Fox (2005). “Rapid evolution and  
 500 the convergence of ecological and evolutionary time”. In: *Ecology Letters* 8.10, pp. 1114–1127.

501 Hiltunen, T., L. E. Jones, S. P. Ellner, and N. G. J. Hairston (2013). “Temporal dynamics of a simple  
 502 community with intraguild predation: an experimental test”. In: *Ecology* 94.4, pp. 773–779.

503 Jia, J. and A. R. Benson (2019). “Neural jump stochastic differential equations”. In: *Advances in*  
 504 *Neural Information Processing Systems* 32.NeurIPS.

505 Jost, C. and S. P. Ellner (2000). “Testing for predator dependence in predator-prey dynamics: A  
 506 non-parametric approach”. In: *Proceedings of the Royal Society B: Biological Sciences* 267.1453,  
 507 pp. 1611–1620.

508 Kendall, B. E. et al. (2005). “Population cycles in the pine looper moth: Dynamical tests of mech-  
 509 anistic hypotheses”. In: *Ecological Monographs* 75.2, pp. 259–276.

510 Lawton, J. H. (1999). “Are There General Laws in Ecology ?” In: *Oikos* 84.2, pp. 177–192.

511 Pearce, T., F. Leibfried, A. Brintrup, M. Zaki, and A. Neely (2018). “Uncertainty in Neural Net-  
 512 works: Approximately Bayesian Ensembling”. In: *arXiv*, pp. 1–10.

513 Pontarp, M., Å. Brännström, and O. L. Petchey (2019). “Inferring community assembly processes  
514 from macroscopic patterns using dynamic eco-evolutionary models and Approximate Bayesian  
515 Computation (ABC)”. In: *Methods in Ecology and Evolution* 10.4, pp. 450–460.

516 Posey, M. H., T. D. Alphin, and L. Cahoon (2006). “Benthic community responses to nutrient en-  
517 richment and predator exclusion: Influence of background nutrient concentrations and interactive  
518 effects”. In: *Journal of Experimental Marine Biology and Ecology* 330.1, pp. 105–118.

519 Raeymaekers, J. A. M. et al. (2017). “Adaptive and non-adaptive divergence in a common land-  
520 scape”. In: *Nature Communications* 8.1, pp. 1–8.

521 Reznick, D. N., H. Bryga, and J. A. Endler (1990). “Experimentally induced life-history evolution  
522 in a natural population”. In: *Nature* 346.6282, pp. 357–359.

523 Rosenbaum, B., M. Raatz, G. Weithoff, G. F. Fussmann, and U. Gaedke (2019). “Estimating param-  
524 eters from multiple time series of population dynamics using bayesian inference”. In: *Frontiers  
525 in Ecology and Evolution* 6.234, pp. 1–14.

526 Shurin, J. B., J. L. Clasen, H. S. Greig, P. Kratina, and P. L. Thompson (2012). “Warming shifts  
527 top-down and bottom-up control of pond food web structure and function.” In: *Philosophical  
528 transactions of the Royal Society of London. Series B, Biological sciences* 367.1605, pp. 3008–  
529 17.

530 Snell, T. W. and B. L. Garman (1986). “Encounter probabilities between male and female rotifers”.  
531 In: *Journal of Experimental Marine Biology and Ecology* 97.3, pp. 221–230.

532 Thompson, C. E., E. B. Taylor, and J. D. Mcphail (1997). “Parallel Evolution of Lake-Stream  
533 Pairs of Threespine Sticklebacks (*Gasterosteus*) Inferred from Mitochondrial DNA Variation”.  
534 In: *Evolution* 51.6, pp. 1955–1965.

535 Wu, J., M. Fukuhara, and T. Takeda (2005). “Parameter estimation of an ecological system by a  
536 neural network with residual minimization training”. In: *Ecological Modelling* 189.3-4, pp. 289–  
537 304.

538 Yoshida, T., S. P. Ellner, L. E. Jones, B. J. M. Bohannan, R. E. Lenski, and N. G. J. Hairston (2007).  
539 “Cryptic population dynamics: Rapid evolution masks trophic interactions”. In: *PLoS Biology*  
540 5.9, pp. 1868–1879.

541 Yoshida, T., L. E. Jones, S. P. Ellner, G. F. Fussmann, and N. G. J. Hairston (2003). “Rapid evo-  
542 lution drives ecological dynamics in a predator – prey system”. In: *Nature* 424.July, pp. 303–  
543 306.



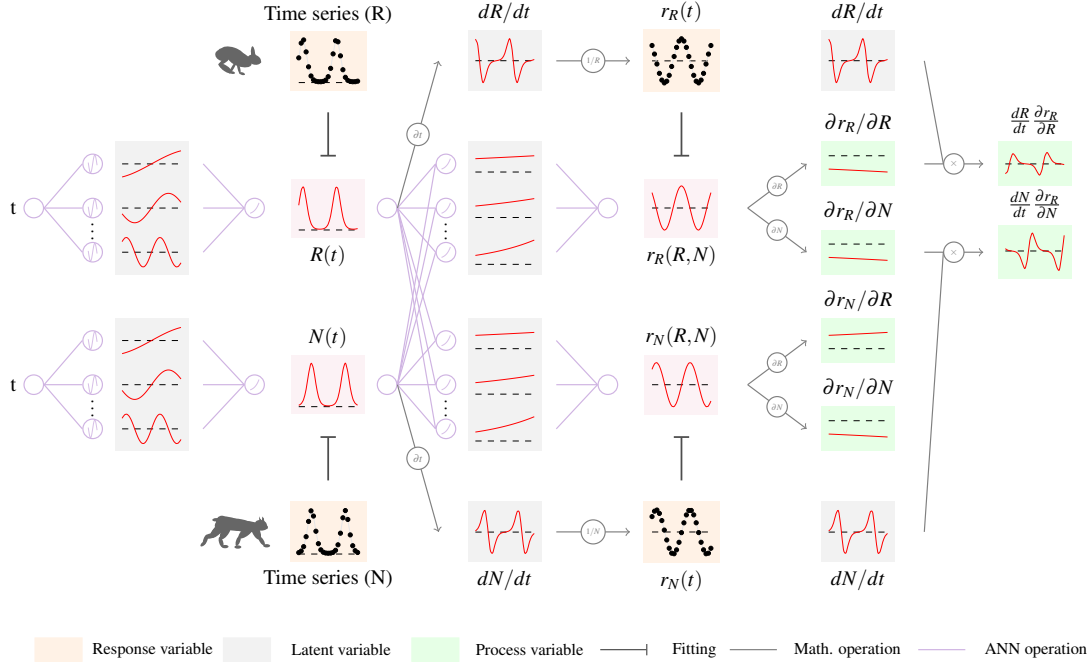


**Figure 1: Overview of fitting neural ordinary differential equations by gradient matching**

The first step is to compute a continuous time approximation (interpolation) of each state variables (e.g. resource  $R(t)$  and predator  $N(t)$ ). To do that we fit an ANN, that takes time as input, to each time series. Dynamics of populations can then be computed by taking the derivative of the ANN with respect to time,  $dR/dt$  and  $dN/dt$ . This provides an interpolation of the per-capita growth rate of each population, e.g.  $r_R(t) = 1/R \, dR/dt$ . In a second step, we approximate non-parametrically the per-capita growth rates with respect to the density of each populations,  $r_R = s(R, N)$ . To do that we fit an ANN, which takes as input the interpolated variables  $R(t)$  and  $N(t)$ , to the interpolated per-capita growth rates  $r_R(t)$  and  $r_N(t)$ . In a final step, we approximate the ecological interactions, by computing the sensitivity of the per-capita growth rates with respect to the density of each population, e.g.  $E : N \rightarrow R = \partial r_R / \partial N$ . We also compute the contribution of each species to the dynamics of the other by multiplying the dynamics of each variable with its effect on the growth rates (i.e. the Geber method), e.g.  $C : N \rightarrow R = dN/dt \times \partial r_R / \partial N$ .

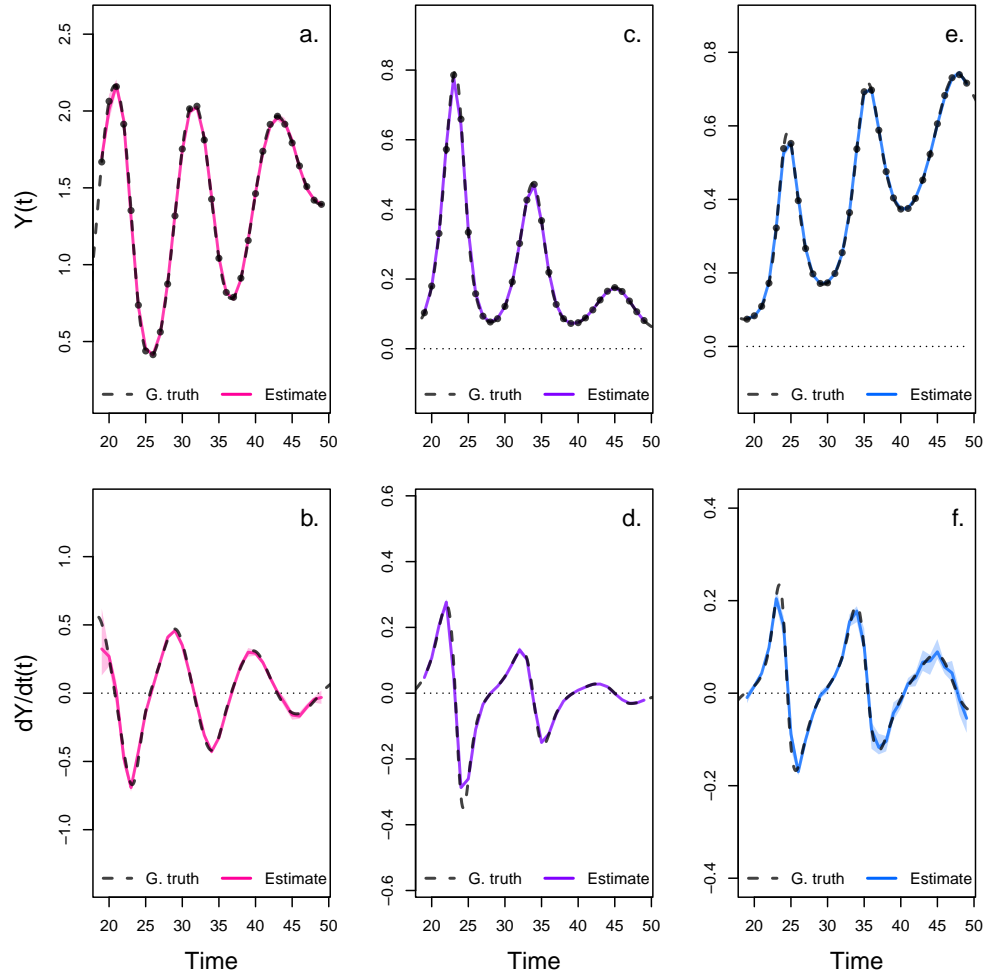


**Figure 2: Interpolated density and dynamics of algae, flagellate, and rotifer in the artificial system.** This figure corresponds to the first step in the overview figure. It shows the accuracy of the interpolated densities of algae (a.), flagellate (c.), and rotifer (e.). We obtain interpolated densities by fitting observed densities (black dots) with ANNs that take time as input. The observed densities were obtained by sampling a tri-trophic prey-predator ODE model at regular time steps. We then derive interpolated dynamics (b., d., f.) by computing the temporal derivative of the interpolated densities with respect to time. In all graphs, the dashed line represents the ground truth, namely trajectories generated by the ODE model. The solid lines correspond to the interpolations. The shaded area shows the 90% confidence interval, obtained by approximately sampling the marginal posterior distributions.

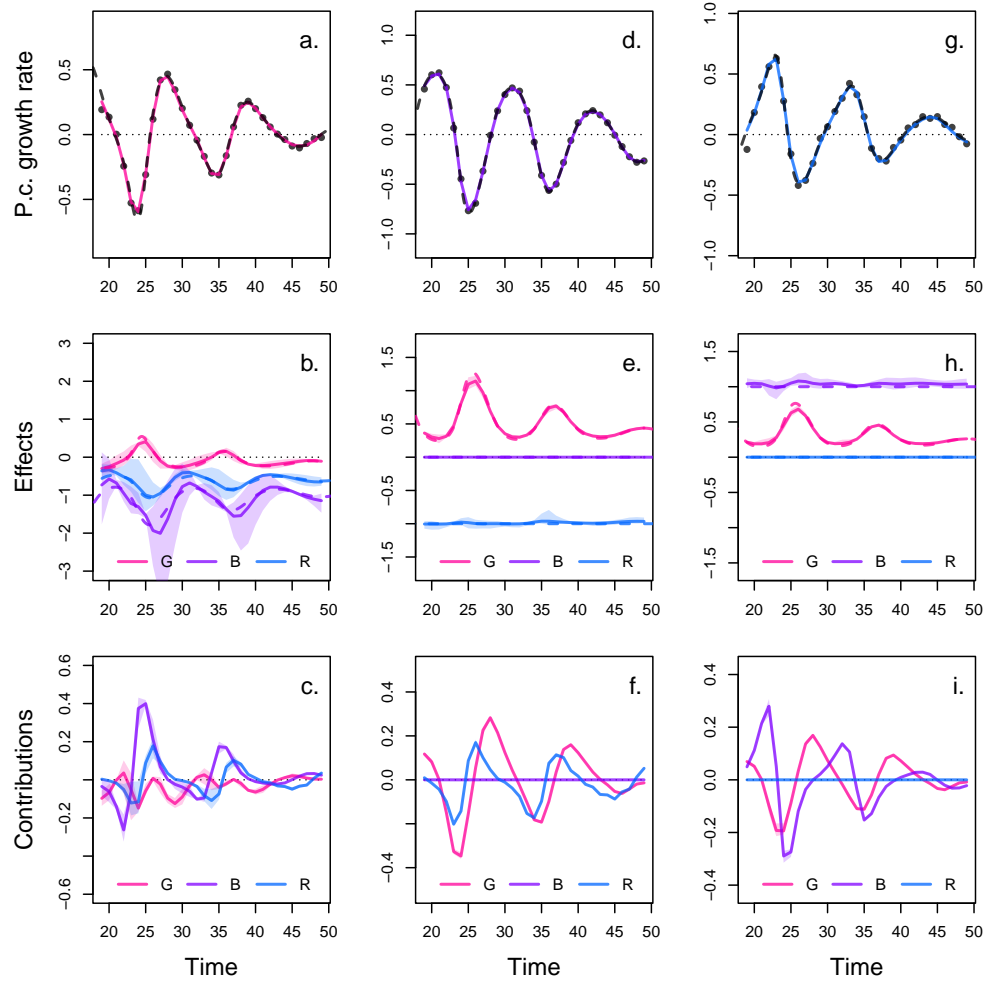


**Figure 3: Drivers of dynamics of algae, flagellate, and rotifer in the artificial system.** This figure corresponds to the second step in the overview figure. It displays the NODE non-parametric approximations of the per-capita growth rate of algae (a., b., c.), flagellate (d., e., f.), and rotifer (g., h., i.). We obtain the NODE approximations (a., d., g., solid line) by fitting the interpolated per-capita growth rates (black dots) with ANNs that take population densities as input. We then estimate the direction of ecological interactions (effects, b., e., h.) by computing the derivative of the NODE approximations with respect to each density. Finally, we compute the strength of ecological interactions (contributions, c., f., i.) by multiplying the interpolated dynamics of each population (fig. 1, b., d., f.) with its effects. Dashed lines correspond to ground truth, obtained from the original trajectories of the tri-trophic ODE model. The shaded area shows the 90% confidence interval, obtained by approximately sampling the posterior distributions.

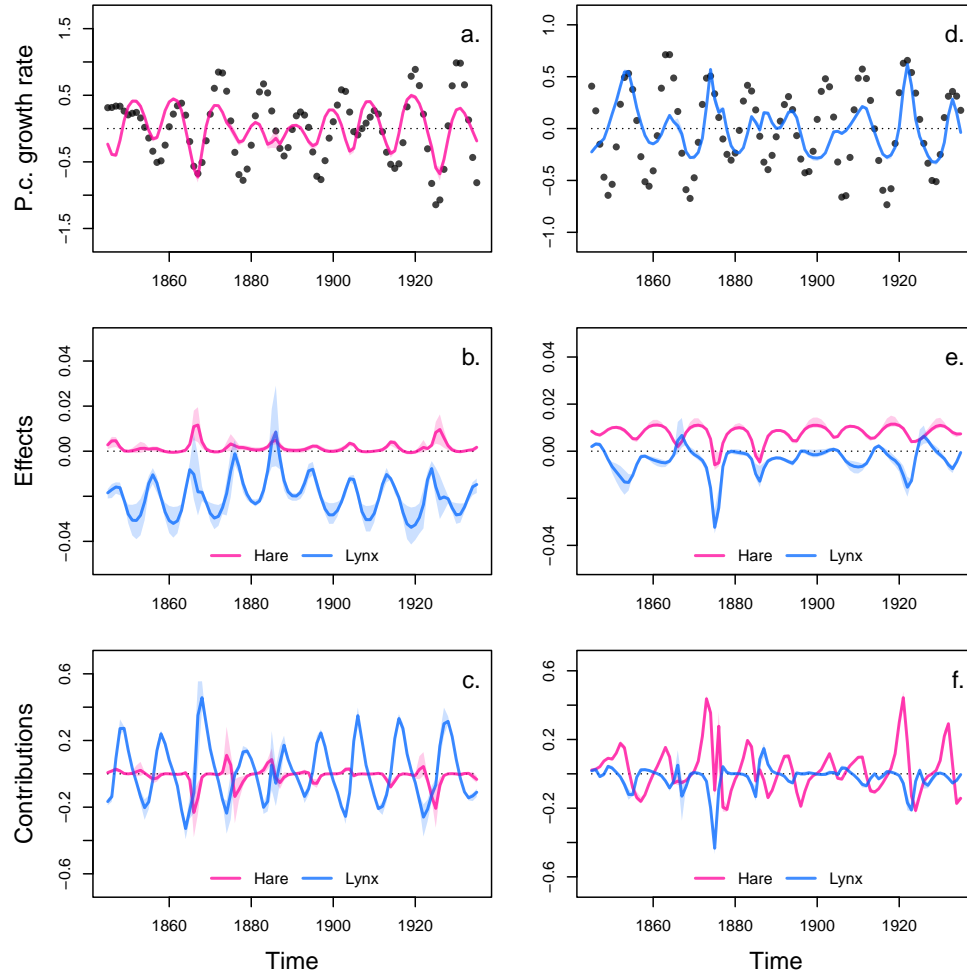


**Figure 4: Drivers of dynamics of hare and lynx in the Odum and Barrett pelt count time series.** This figure displays the NODE non-parametric approximations of the per-capita growth rate of hare (a., b., c.), and lynx (d., e., f.). We obtain the NODE approximations (a., d., solid line) by fitting the interpolated per-capita growth rates (black dots) with ANNs that take population densities as input. We then estimate the direction of ecological interactions (effects, b., e.) by computing the derivative of the NODE approximations with respect to each density. Finally, we compute the strength of ecological interactions (contributions, c., f.) by multiplying the interpolated dynamics of each population with its effects. The shaded area shows the 90% confidence interval, obtained by approximately sampling the posterior distributions.

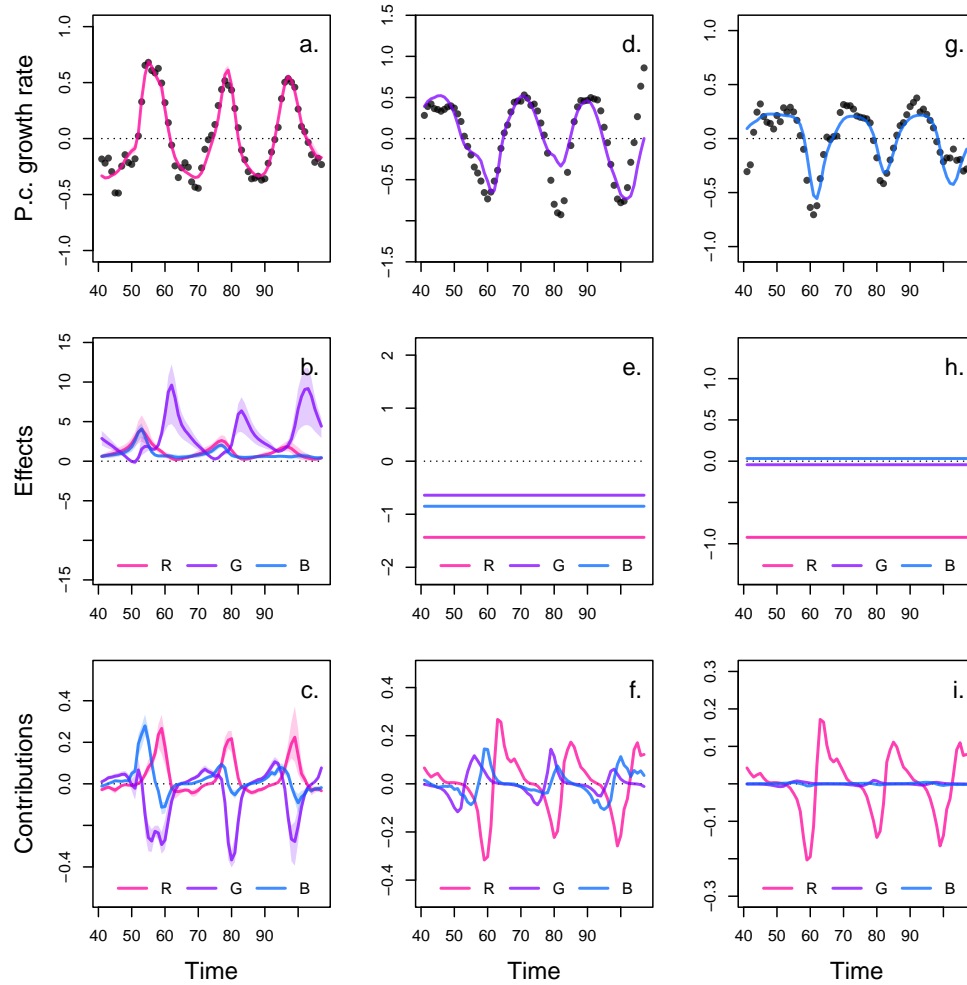


**Figure 5: Drivers of dynamics of algae, flagellate, and rotifer in replicate A.** This figure displays the NODE non-parametric approximations of the per-capita growth rate of algae (a., b., c.), flagellate (d., e., f.), and rotifer (g., h., i.). We obtain the NODE approximations (a., d., g., solid line) by fitting the interpolated per-capita growth rates (black dots) with ANNs that take population densities as input. We then estimate the direction of ecological interactions (effects, b., e., h.) by computing the derivative of the NODE approximations with respect to each density. Finally, we compute the strength of ecological interactions (contributions, c., f., i.) by multiplying the interpolated dynamics of each population with its effects. The shaded area shows the 90% confidence interval, obtained by approximately sampling the posterior distributions. The replicated time series were obtained by digitising the time series in Hiltunen et al. (2013).

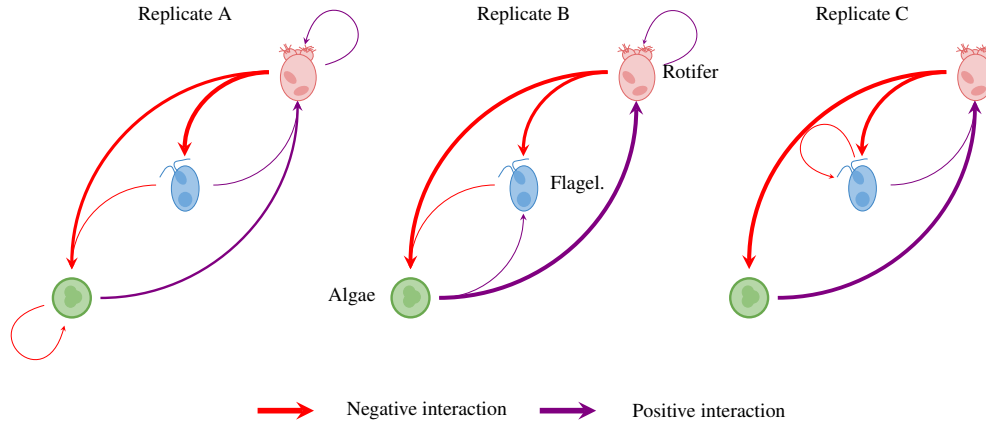


**Figure 6: Interaction networks inferred from 3 replicated time series of algae, flagellate, and rotifers.** This figure shows the direction and strength of ecological interactions inferred from 3 replicated sets of time series of algae, flagellate, and rotifer, using NODEs fitted by gradient matching. The replicates B and C were analysed in the same way as replicate A (see fig. 5 for details). Red and purple arrows correspond to negative or positive mean effects. We estimated mean effects by averaging effects (i.e. derivative of NODE approximated per-capita growth rates with respect to each population density) across the time series. The width of the arrows is proportional to the relative strength of the ecological interaction. We compute the relative strength as the % of total contributions attributable to either algae, flagellate, or rotifer, obtained from summing the square of contributions of each species throughout the time series. For instance in replicate A, the relative strength of the effect of rotifer on algae is found by summing the square of the red line in fig. 5 f., and computing the % of total contributions that it accounts for. We provide the value of the mean effects and relative strengths in Table 1. The replicated time series were obtained by digitising the time series in Hiltunen et al. (2013).

**Table 1: Summary analysis.**  $r^2$  corresponds to the r squared of the NODE non-parametric approximation of the pre-capita growth rate compared to the interpolated per-capita growth rate for each of the three species. Mean effects are obtained by averaging the effect of one species on the growth rate of another throughout the time series. The % of total contributions is obtained by summing the square of contributions of one species density to the growth of the other at each time step throughout the time series, then by computing the proportion of total change that it accounts for.

		R	G	B
<b>replicate A</b>				
<b>Mean effects</b>	on R	0.27	0.77	0.97
	on G	-1.17	-0.44	-0.85
	on B	-0.78	0.04	0.03
<b>% of total contributions</b>	to R	0.08	0.48	0.44
	to G	0.75	0.08	0.17
	to B	1	0	0
<b>replicate B</b>				
<b>Mean effects</b>	on R	0.08	0.59	0.22
	on G	-1	0.05	-0.48
	on B	-0.47	0.14	-0.02
<b>% of total contributions</b>	to R	0.02	0.93	0.05
	to G	0.9	0	0.1
	to B	0.9	0.1	0
<b>replicate C</b>				
<b>Mean effects</b>	on R	-0.1	0.45	0.93
	on G	-1.76	-0.13	-0.12
	on B	-0.76	0.01	0.08
<b>% of total contributions</b>	to R	0.01	0.31	0.67
	to G	0.99	0.01	0
	to B	0.99	0	0.01

## 544 6 Supplementary

### 545 A Bayesian regularisation

546 The fitting of the models is performed in a Bayesian framework, considering normal error structure  
547 for the residuals, and normal prior density distributions on the parameters

$$p(\theta|\mathcal{D}) \propto p(\mathcal{D}|\theta)p(\theta) \quad (13)$$

548 where  $\theta$  is the parameter vector of the model, and  $\mathcal{D}$  the evidence, namely the data that the model  
549 is fitted to. Assuming a normal likelihood for the residuals given the evidence we get

$$p(\mathcal{D}|\theta) = \prod_{i=1}^I \frac{1}{\sqrt{2\pi\sigma^2}} \exp \left\{ -\frac{e_i(\mathcal{D}, \theta)^2}{2\sigma^2} \right\} \quad (14)$$

550 where  $e_i(\mathcal{D}, \theta)$  are the residuals of the model given the parameters, and the evidence. In the case of  
551 the interpolation, the residuals correspond to the observation error  $\varepsilon^{(o)}$  (equation 3). In the case of  
552 the NODE approximation, they correspond to the process error  $\varepsilon^{(p)}$  (equation 7).  $I$  is the number  
553 of data points, either observations in the case of the interpolation, or interpolated points in the case  
554 of the NODE fitting.

555 The prior probability density functions for the parameters are given by

$$p(\theta) = \prod_{j=1}^J \frac{1}{\sqrt{2\pi\delta_j^2}} \exp \left\{ -\frac{\theta_j^2}{2\delta_j^2} \right\} \quad (15)$$



where  $J$  is the number of parameters in the models. The parameter  $\delta_j$  controls the dispersion of the priors, and thereby the complexity/level of constraint of the model.

There is no standard approach for choosing  $\delta$ . Low values of dispersion may increase constraint on parameters too drastically, which would lead to underfitting, and result in a reduction of the variance of parameter estimates and bias mean estimates towards 0. In contrast, too high values of dispersion may lead to overfitting, by allowing for more complex shapes. To account for this, we optimise the models on the second-level of inference. This means that we are finding the optimal value of  $\delta$ , in addition to optimising the model parameters. We do this by optimising the marginal posterior density of the parameters, obtained by averaging out  $\delta$  following a modification of the approach developed by Cawley and Talbot (Cawley and Talbot 2007). This yields the following expression for the marginal log posterior density of the parameters

$$\log P(\Omega|\mathcal{D}) \propto -\frac{I}{2} \log \left( 1 + \sum_{i=1}^I \left( \varepsilon_i^{(o)} \right)^2 \right) - \frac{J}{2} \log \left( 1 + \sum_{j=1}^J \Omega_j^2 \right) \quad (16)$$

$$\log p(\beta|\Omega) \propto -\frac{1}{2} \sum_{i=1}^I \left( \frac{\varepsilon_i^{(p)}}{\sigma} \right)^2 - \frac{1}{2} \sum_{j=1}^J \left( \frac{\beta_j}{\delta_j} \right)^2 \quad (17)$$

which amounts to optimising the log of the sum of squared residuals rather than the sum of squared residuals.  $P(\theta|\mathcal{D})$  designates the marginal posterior distribution. More details on how to derive this expression from equation (8) can be found in a supplementary file (See supplementary A).

In this section we describe how to derive the modified model selection criteria developed by Caw-

ley and Talbot (Cawley and Talbot 2007). Bayesian regularisation simply amounts to constraining  
 the values of the parameters in the model to be close to a desired value. Usually, parameters are  
 constrained by choosing normal priors centered about 0. In this case, the standard deviation of the  
 normal priors governs the range of values that the parameters can take, and hence constrains more  
 or less strongly the behaviour of the model (Cawley and Talbot 2007). Performing inference on the  
 second level means that we are trying to find the appropriate value of the dispersion of the priors,  
 in other words, the appropriate level of constraint on the model. In practice, choosing the level of  
 constraint is difficult, Cawley and Talbot hence developed a criterion to perform model selection  
 on the second level of inference. They proposed to optimise the marginal posterior distribution by  
 averaging out the dispersion of the priors. With an appropriate choice of prior, the dispersion can  
 be integrated out, leaving us with a formula for the posterior that only depends on the parameters  
 of the model,

$$\log P(\theta|\mathcal{D}) \propto -\frac{I}{2} \log \left( \sum_{i=1}^I e_i(\mathcal{D}, \theta)^2 \right) - \frac{J}{2} \log \left( \sum_{j=1}^J \theta_j^2 \right) \quad (18)$$

where  $P(\theta|\mathcal{D})$  denotes the marginal posterior density,  $\mathcal{D}$  denotes the evidence,  $I$  and  $J$  denote the  
 number of data points and parameters, respectively,  $e_i$  denote the residuals of the model, and  $\theta$   
 denote the parameters of the model. The construction is elegant because it is not sensitive to the  
 choice of prior hyperparameters, and simple as it amounts to optimising the log of the sum of  
 squares, rather than the sum of squares (in the case of normal ordinary least square).

588 The issue with this formula is that the marginal posterior density is infinity when the parameters  
 589 are 0, which leads to underfitting. In this paper we use a modified criterion, which corrects for that  
 590 problem

$$\log P(\theta|\mathcal{D}) \propto -\frac{I}{2} \log \left( 1 + \sum_{i=1}^I e_i(\mathcal{D}, \theta)^2 \right) - \frac{J}{2} \log \left( 1 + \sum_{j=1}^J \theta_j^2 \right) \quad (19)$$

591 where the marginal posterior density depends only on the residuals of the model when the parame-  
 592 ters are equal to 0, and otherwise depends on both the parameters and the residuals. This construc-  
 593 tion can be obtained simply by assuming a gamma prior for the parameters  $p(\xi) \propto \frac{1}{\xi} \exp\{-\xi\}$ ,  
 594 where  $\xi$  is the regularisation parameter, instead of the improper Jeffreys' prior that Cawley and  
 595 Talbot used in their original study, namely  $p(\xi) \propto \frac{1}{\xi}$ . The details of the integration of the posterior  
 596 distribution over  $\xi$  can be found in Cawley and Talbot's original paper.